http://dx.doi.org/10.21611/qirt.1994.033

Thermal defectometry using the temperature decay rate method

by DELPECH P.M.*, KRAPEZ J.C. and BALAGEAS D.L.

L3C, ONERA, BP 72 F-92322 Châtillon-Cedex, France.

** University of Bath, School of Materials Science, Claverton Down, Bath BA2 7AY, Avon, United Kingdom.*

Abstract

The pulsed stimulated infrared thermography NDE method has been used to evaluate the integrity of thin structures in highly conductive materials. An inversion procedure for the thermal images is obtained from an analytical solution of the 1D heat transfer through a bilayer including a thermal resistance at the interface with third kind conditions on its external boundaries. A simplified analytical model is suitable for long time inspection and allows the identification of both the depth location and the thickness of the defects without any previous experiment on a reference sample. 2D effects are studied by inversion of numerically calculated thermograms. Experimental analysis of samples made of metallic materials used in aircraft construction are presented.

NOMENCLATURE

a	diffusivity ($m^2.s^{-1}$)	t	time (s)
e	total thickness of the sample (m)	R	thermal resistance ($m^2.KW^{-1}$)
e_1, e_2	thickness of layer 1, 2 (m)	R*	dimensionless thermal resistance (kR/e)
h	heat loss coefficient ($W.m^{-2}.K^{-1}$)	Q	fluence ($J.m^{-2}$)
h_R	heat transfer coefficient ($W.m^{-2}.K^{-1}$)	z	depth (m)
C	volumetric heat capacity ($J.m^{-3}.K^{-1}$)	z*	dimensionless depth ($=e_1/e$)
k	thermal conductivity ($W.K^{-1}.m^{-1}$)	α_n	eigenvalue (m^{-1})
T_i	temperature (K)	β_m	parameter (K or s^{-1} if m is odd or even)
T∞	adiabatic temperature (K)	τ	pulse duration (s)

1. Introduction

Most of the work which has been done until now in academic and industrial research centers to improve the Stimulated Infrared Thermography nondestructive evaluation technique seems mainly oriented toward low conductivity materials. This situation is due to the industrial requirements in nondestructive testing (NDT). One of these requirements was to provide a suitable NDT method for the wide range of new composite materials which are imperfectly covered by more traditional NDT techniques. These composites are made of poor thermal conductivity materials like epoxy or glass matrix based composites for example. The consequences of these efforts are that the experimental implementation of the technique and its industrial applications are well known. The new comer to the technique can find a lot of valuable information in the literature on both theoretical and practical aspects of the problem. In the particular case of the low conductivity materials, the quantitative identification of defects has been extensively investigated by a large amount of previous work. Reliable models of the experimental procedures and the inversion procedures for transient thermal images have been tested and are available for use in the field [1, 2, 3].

In our laboratory, we paid a particular attention to other kinds of materials like carbon-carbon composites which are of great interest for high temperature aerospace applications [4]. We also have been interested in the more classical problem of evaluation of adhesive bonds between aluminum alloys plates [5] which are widely used in aircraft structures. For this purpose, we used a classical pulsed thermographic experimental set-up involving a powerful radiative excitation source (controlled by a mechanical shutter) coupled with an IR imager

*The colour plates of this article are on page **XIII** at the end of the book.*

http://dx.doi.org/10.21611/qirt.1994.033
whose signal is digitized in real-time and stored in a micro-computer. A reflection configuration has been preferred (excitation and detection are located on the same face) because of the more general application possibilities. The transient signal received by the camera from the sample following excitation is recorded and analyzed.

The high conductivities of aluminum alloys and carbon-carbon materials imply that the known methods for identification of inclusions which uses the thermal contrast (temperature difference between a flawed and an unflawed area) are not readily applicable. This is due to the pulse duration time of real radiative excitation sources being comparable to that of the subsequent thermal transients in these high conductivity materials.

To solve this problem we developed a 1 Dimensional model for defect in a sample. From this we obtained an identification procedure which makes use of actual thermal transient, rather than the thermal contrasts used in other methods. The analytical model established is firstly presented in this paper and the meanings of the main parameters are highlighted. Then the data inversion procedure used is described. The limitations of the method are investigated by applying it to thermograms obtained from a 2D numerical simulation of the heat flow through a sample containing a finite defect. Finally experimental results are presented and discussed.

2. Analytical 1D model.

2.1. Front face temperature of the bilayer after the heat pulse.

Let us consider a two layer sample of total thickness e (figure 1). An imperfect thermal contact at the interface, located at a depth e_1 is modeled by a thermal contact resistance R (or the equivalent transfer coefficient $h = 1/R$). The sample received a heat fluence Q of duration τ on its front face and is subject to heat losses on its two faces. The heat losses are characterized by an equal coefficient h on both sides. We solved this 1D conduction problem using the classical method of separation of variables which leads to the following expression for the front face temperature for $t > \tau$ [4] :

$$T(t) = \sum_{n=1}^{\infty} T_n(t) = \sum_{n=1}^{\infty} T_\infty \frac{4\, e\alpha_n}{\text{Denominator}} \frac{\exp(a\alpha_n^2\tau) - 1}{a\alpha_n^2\tau} \exp(-a\alpha_n^2 t) \qquad (1)$$

$$\text{Denominator} = \left(1+\left(\frac{h}{k\alpha_n}\right)^2\right)2\alpha_n e_1 + \left(1-\left(\frac{h}{k\alpha_n}\right)^2+2\frac{h}{k\alpha_n}tg(\alpha_n e_1)\right)\sin(2\alpha_n e_1) +$$

$$\left(\frac{\frac{h}{k\alpha_n}\cos(\alpha_n e_1) - \sin(\alpha_n e_1)}{\sin(\alpha_n e_2) - \frac{h}{k\alpha_n}\cos(\alpha_n e_2)}\right)^2 \left[\left(1+\left(\frac{h}{k\alpha_n}\right)^2\right)2\alpha_n e_2 + \left(1-\left(\frac{h}{k\alpha_n}\right)^2+2\frac{h}{k\alpha_n}tg(\alpha_n e_2)\right)\sin(2\alpha_n e_2)\right]$$

which is an infinite series where $T_\infty = Q/Ce$ would be the temperature reached by the sample at a very long time with no heat losses and where the values α are, in the general case, the positive roots of the transcendental equation :

$$\frac{k\alpha}{h_R} = \cot g\left(\alpha e_1 - \text{Arctg}\frac{h}{k\alpha}\right) + \cot g\left(\alpha e_2 - \text{Arctg}\frac{h}{k\alpha}\right) \qquad (2)$$

This transcendental equation can be solved graphically (figure 2). The eigenvalues α_n are then given by the intersection of a straight line ($k\alpha/h_R$) and a periodic curve $f(\alpha)$ versus α. The figure 2 shows two sets of asymptotes as1 and as2 for the periodic curve, whose positions on the horizontal axis are determined by the thickness of each of the layers, e_1 and e_2 :

$$tg\,\alpha e_1 = \frac{h}{k\alpha} \quad \text{or} \quad tg\alpha e_2 = \frac{h}{k\alpha} \qquad (3)$$

A particular case occurs when, owing to the thickness of the layers and the external boundary conditions, two asymptotes are superimposed. The eigenvalue generally located between the two asymptotes is therefore given by the equations (3).

http://dx.doi.org/10.21611/qirt.1994.033

It is also important to notice that the eigenvalues are totally independent of the initial conditions and are only related to the internal and external boundary conditions. Moreover in the case of natural convective heat losses at the external boundaries, the first eigenvalue is very low and, in addition, tends to zero when the heat loss coefficient h approaches zero. Therefore the first term of the infinite series (1) tends to T_∞ when the heat losses are negligible. The following terms in the series and the corresponding transcendental equation are readily derived from (1) and (2) by setting h=0.

The influence of the initial excitation (square pulse here) appears in the expression (1) in the multiplicative fraction which involves the pulse length τ. This fraction becomes one as the length of the pulse approaches zero. Thus, the solution for a Dirac excitation is directly obtained from expressions (1).

2.2 Influence structure.

For a thin and high thermal conductivity sample one verifies that expression (1) converges towards the sum of the two first terms, corresponding to a very short time after the excitation pulse. A simplified expression of the temperature T(t) then has the form :

$$T(t) = \beta_1 \exp(-\beta_2 t) + \beta_3 \exp(-\beta_4 t) \quad (4)$$

A variational study of the four parameters β (m=1,2,3,4) versus the variables of interest R, e_1 and h shows the physical significance of these parameters. As expected, β_1 and β_2, which are function of the first eigenvalue α_1, are weakly dependent on the defect. β_2 is strongly linked to variations of the heat losses. On the other hand, the parameters β_3 and β_4 (proportional to the second eigenvalue α_2) are sensitive to the depth location and to the thermal resistance of the defect, respectively.

The predicted magnitude of the thermal contrast, following the heat deposition, due to a defect can be used to investigate the influence of the four parameters. Here, the contrast due to the defect is easily assessed since the eigenvalues corresponding to the reference temperature (unflawed area) can be calculated by the same expression (2) with left side equal to zero. Actually, in this case, the contrast can be seen in figure 2 as a shift between the eigenvalue α_2 and the intersection of the periodic curve and the horizontal axis.

3. Identification procedure.

3.1. Main steps of the inversion procedure.

An example of the application of a data inversion procedure based on the above analysis is presented here. The application is the identification of an air gap between two metallic plates. The experimental sample used was a bilayer made of two 1mm steel plates (k = 55 W/mK, $C=3{,}616.10^6$ J/m^{3}K, e = e_1+e_2 = 1+1 mm ± 0,034 mm). The two plates were held by their edges in order to leave a thin layer of air between them (h_R>500 SI). The sample receives a radiative square pulse on its front face (τ =0.8s). The temperature transient of the same face was recorded by the camera.

We will not develop here a complete description of the two different parameter estimation procedures used to identify the parameters β. The first one is a classical Non-Linear Least Square Method (Levenberg-Marquardt) [6]. This method can deal with the four parameter model but has only been implemented for one recorded pixel point. The second method which involves weighted temporal integrals of the signal has been described previously [5]. This method, adapted to the three parameter model (heat losses are neglected β_2=0) is faster in implementation and is preferred for full image inversions.

The temporal evolution of the temperature after the pulse ($t>\tau$) and the result of the curve fitting procedure by the four parameters Least Square method are shown in figure 3. The identified components of the array [β] are :

$$[\beta] = [518{,}7 \quad 6{,}2.10^{-3} \quad 594{,}3 \quad 0{,}433]$$

http://dx.doi.org/10.21611/qirt.1994.033

The physical parameters of the experimental system can be estimated sequentially from these values of [β] :

- β_2 gives α_1 which allows the identification of the heat losses coefficient h by using the transcendental equation related to the case of a monolayer structure of total thickness e.

- then one can calculate the adiabatic temperature T_∞ (in arbitrary units N chosen to suit the measurement system, but proportional to the temperature) from β_1 in which α_1 and h are known (the value of e_1 is not critical and can be assumed equal to e/2).

- hence all the variables involved in the theoretical expression of β_3 are then known except for the depth of the interface e_1 (the quantity T_∞ contains all the information about the spatial dependence of the excitation pulse energy received by the sample and the sample surface emissivity). An iterative determination of e_1 can be performed. Starting with the value $e_1 = e/2$ the iteration is stopped when two successive values are close enough. In practice, a few iterations (about five) are sufficient for a convergence better than 10^{-3}.

- finally, the thermal resistance R is simply given by the relation (2).

In our example, these four steps lead to the following results :

h = 22,3 SI, T_∞ = 517,5 N, e_1 = 1,02 mm and h_R = 778,3 SI (32,1 µm of air)

e_1 is in very good agreement with the known interface depth of 1mm. The measurements of the thickness of the air gap has been made with a feeler gage which gave the value 25µm±15µm, which encompasses the value obtained for h_R.

We also indicate the results obtained with the same estimated parameters (from array β) by assuming that the two metallic plates only acts as heat capacitors (see [5] for more details about this model):

e_1 = 1,02 mm, h_R = 782,1SI (32,0µm of air)

It is interesting to notice the similarity of the values given by the two models. This similarity actually highlights the physical meaning and the relevance of the simplification made in the first model (expression 7). More precisely, the transient response is mainly governed by the heat flow through the thermally resistant interface. The thermal conduction, caused by the thermal gradient in the two layers, appears here as a second order phenomenon (the infinite series in the complete analytical expression for the temperature comes from the conduction phenomenon). This phenomenon is ignored in the capacitive model which is a limiting case of the exact model obtained by setting the thermal conductivity to an infinite value.

This type of comparison can be used to determine whether the capacitive model is acceptable or not for a particular application. For example if a 5% uncertainty is acceptable the capacitive model can be used for evaluation of bilayers with interfaces located between z^*=0.1 and 0.8 provided the thermal resistance R^* is over 10. For the previous steel bilayer, the expected thermal resistance laid between 11 and 44, so the capacitive model is justified and a more sophisticated treatment is no longer needed.

3.2. The influence of 2D effects on the inversion procedure results.

The ideal interface included in the bilayer test-piece studied is far from being representative of a real interface in a bounded structure. One of the most probable limitations of this 1D model, and its application to the identification of failures in structures, is the validity of its 1D assumption. We investigated this limitation by using a numerical calculation of the temperature above a finite circular defect located at the interface. The temporal evolution of the front face temperature was calculated along a radial line starting from a point located above the center of the defect to a point above the unflawed area. This latter point was far enough from the defect edge to assume that it was over a region of 1D heat flow. Figure 4 shows the temporal temperature evolution of three points which are located above the defect (middle and edge) and above the unflawed area.

The 1D data reduction procedure previously described, was applied for each point along the radial line. Figure 5 shows an example of spatial dependence of the identified parameters β_3 and β_4. This dependence is quite significant and provides a good quantitative means of detecting a flawed area. The half maxima of these curves do not occur directly above the

http://dx.doi.org/10.21611/qirt.1994.033
defect edge ($r^*=1$) but around $r^* \cong 1.2$. However, this could be used as a first order defect sizing approximation in an automated image inversion procedure. The percentage errors in defect depth and thermal resistance found by applying the 1D inversion procedure to the simulated 2D data are shown in figure 6. These errors are an underestimate of lower than 5% for $r^*<0.5$. Near the edge of the defect, the errors in thermal resistance become larger and the defect depth is strongly overestimated.

4. Application to failure detection inside a metallic bond

The sample was made of two imperfectly bonded aluminum plates. The front face was black painted and received a pulse of 2s duration. The data reduction procedure was applied with each pixel of the successive thermal images obtained after pulse heating. The color image presented in figure A can be regarded as being a graphical representation of the state of the interface. This evaluation is quantified in terms of thermal resistance. The central lowest value corresponds to the fully bonded part of the joint, and the highest values are due to air gaps at the edges. Due to the small area of the test-sample the 1D assumption is not valid. The magnitude of the thermal resistance values above the air gaps are about half what would be expected whereas those for the bounded part are larger by a factor of two. However, despite this bias in the quantitative results, the extent of the bounded area is accurately identified.

5. Conclusions

The quantitative evaluation method proposed in this paper is quite simple and suitable for thin high conductive structures. The 1D assumption of the model is its main theoretical limitation. However, we verified the reliability of the quantitative identifications performed in several practical cases. A higher level of confidence could be reached if the identification was coupled with a direct 2D numerical calculation. Such a calculation would be used to preview the expected deviations caused by 2D heat diffusion effects. The rapidity of the stimulated infrared thermography NDE technique coupled with this efficient quantitative inversion method has potential to solve many industrial problems which are time-consuming for alternative NDE techniques. The evaluation of aging aircraft structures is such a problem.

Acknowledgments

The authors are grateful to Dr D. P. Almond, from Bath University, for his participation in the preparation of this paper.

REFERENCES

[1] BALAGEAS (D.L.), DÉOM (A.A.) and BOSCHER (D.M.), *Characterization and nondestructive testing of carbon-epoxy composites by a pulse photothermal method*, in *Materials Evaluations*, 45, 461-465, 1987.

[2] KRAPEZ (J.-C.), MALDAGUE (X.) and CIELO (P.), *Thermographic Nondestructive Evaluation: Data Inversion Procedures : Part I - 1-D Analysis. Part II - 2-D Analysis and Experimental Results* in *Research in Nondestructive Evaluation* 3, 1991

[3] MAILLET (D.),HOULBERT (A.S.), DIDIERJEAN (S.), LAMINE (A.S.) and DEGIOVANNI (A.), *Non-destructive thermal evaluation of delaminations in a laminate : Part I - Identification by measurement of thermal contrast. Part 2 - The experimental Laplace transforms method.* in *Composites Science and Technology*, no 47, 1993.

[4] DELPECH (P.M.) *Contrôle non destructif par thermographie infrarouge des structures composites chaudes d'Hermès*, Thesis (in french), Ecole Centrale de Nantes, 1993.

[5] DELPECH (P.M.), BOSCHER (D.M.), LEPOUTRE (F.), DÉOM (A.A.) and BALAGEAS (D.L.), *Non destructive evaluation of adhesive bonds by pulse-stimulated infrared thermography* in *Review of Progress in Quantitative NDE*, edited by D.O. Thompson and D.E. Chimenti (Plenum Press, New York, 1992), Vol. 11A, pp. 465-470.

[6] PRESS (W.H.), FLANNERY (B.T.), TEUKOLSKY (S.A.) and VETTERLING (W.T.), *Numerical Recipes*, Cambridge University Press, 1986

http://dx.doi.org/10.21611/qirt.1994.033

FIGURES

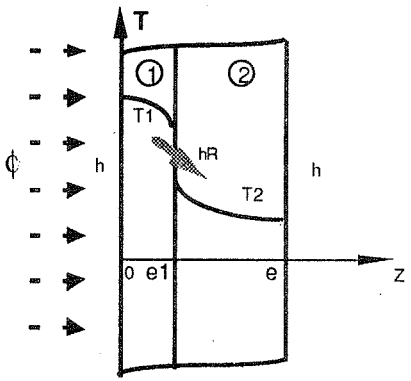

Fig. 1. - 1D model of a two layer sample with imperfect contact at the interface located at depth e_1.

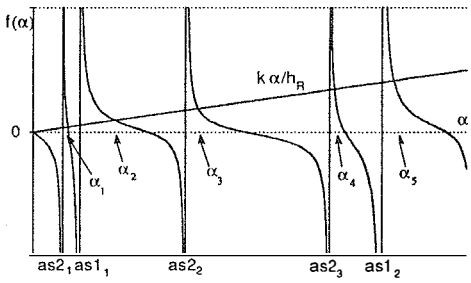

Fig. 2. - Graphical solution of the transcendental equation.

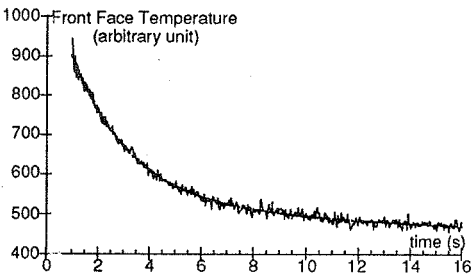

Fig. 3.- Experimental temporal evolution of the front face temperature of a steel bilayer following the heat pulse (spatial average 49pixels).

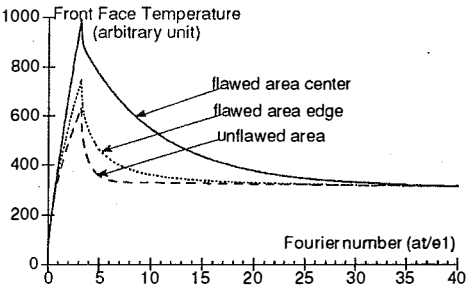

Fig.4.- Temporal evolution of the front face temperature of a bilayer, above the centre and the edge of a finite defect and above an unflawed area.

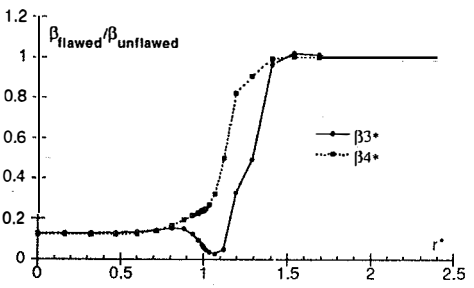

Fig. 5.- Spatial evolution of the parameters β_3 and β_4 versus the normalized radius of the defect (edge of the defect located at r*=1).

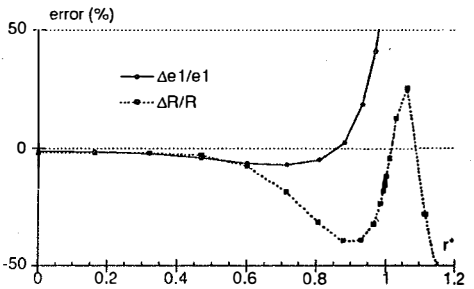

Fig.6.- Errors $\Delta e_1/e_1$ et $\Delta R/R$ versus the normalized radius of the defect (edge of the defect located at r*=1).